When does vapor pressure deficit drive or reduce evapotranspiration?

A. Massmann[1], **P. Gentine**[1], **C. Lin**[2]

[1]Department of Earth and Environmental Engineering, Columbia University, New York, NY 10027

[2]Department of Hydraulic Engineering, Tsinghua University, Beijing, CN

Key Points:

- = enter point 1 here =
- = enter point 2 here =
- = enter point 3 here =

Corresponding author: Adam Massmann, akm2203@columbia.edu

Abstract

= enter abstract here =

1 Introduction

← This section needs to be fleshed out, and I definitely need to add more citations

Changes to vapor pressure deficit (VPD) alter the atmospheric demand for water from the land surface. Traditionally, atmospheric scientists and hydrometeorologists generally think that an increase in atmospheric demand induces an increases in evapotranspiration (ET) (citations?). This possible misconception developed in part due to the proliferation of studies examing potential ET (PET) rather than estimates of ET itself (citations?). In contrast, plant physiologists know that stomata have evolved to optimally regulate the exchange of water and carbon, and tend to close in response to increased atmospheric dryness [**???**]. Therefore, an increase (decrease) in VPD may not correspond to an increase (decrease) in ET because stomatal closure (opening) can cancel the effects of shifts to atmospheric demand.

Quantifying the plant response to a perturbation to atmospheric VPD increases our understanding of land surface response to shifts in atmospheric conditions. If plant response reduces ET in response to atmospheric drying then soil moisture will be conserved. An increase in ET in reponse to atmospheric drying will reduce soil moisture, but contribute increased moisenting to the atmosperhere. Clearly, the sign and magnitude of land-surface responsedrives the co-evolution of the atmosphere and land-surface at many timescales, from diurna to interdecadal.

We hypothesize that for most plant types a common resonse to increase in VPD will actually be a decrease in ET. The excpetion would be plants such as crops that are evolved (or bred) to prioritize gross primary production (GPP) over water conservation. However, for all otehr plants types, our hypothesis calls into question the validity of PET-based drought metrics deceloped by hydrometeorologists and used extensively in operations [e.g. PDSI, P-PET, **??**] . These metrics ignore the role of plants as gatekeepers for surface water loss to the atmosphere and have limited physical meaning for drought of vegetated land types. Additionally, plants evolved in arid climates should prioritize water conservation and we would expect a very negative ET response to increase in VPD. Therefore, vegetated locations most likely to experience droughts should show the strongest deviation between reality and a PET-based approximation.

← more citations needed, including recent PET climate studies like Jack Scheff

In order to quantify plant response to perturbations to atmospheric demand for water, we apply a Penman-Monteith framework to eddy-covariance observations spanning various biomes and climates. Section 2 describes the data used, Section 3 derives the framework, Section 4 presents results, and Section 5 discusses conclusions. The goal of this paper is to use reasonable approximations as a tool to increase intuition for plant response to atmospheric drying. This intuition will aid interpretation of observations and full complexity climate models.

2 Data

We use data from FLUXNET2015. Because g_1 coefficients [**?**] and uWUE were only both available for five plant functional types (PFTs - see Table 3), only 56 of the 77 sites were used. Figure 1 presents each site and its plant functional type.

← map needs to be improved - it's a placeholder for now

3 Methods

n The Penman-Monteith equation (hereafter PM) estimates ET as a function of atmospheric and land-surface variables:

$$ET = \frac{\Delta R + g_a \rho_a c_p D_s}{\Delta + \gamma(1 + \frac{g_a}{g_s})}, \tag{1}$$

where variable definitions are given in Table 1. **?** developed a model for g_s by combining optimal photosynthesis theory with empirical approaches. The result for leaf-scale stomatal resistance was:

$$g_{l-s} = g_0 + 1.6\left(1 + \frac{g_1}{\sqrt{D_s}}\right)\frac{A}{c_s} \tag{2}$$

This can be adapted to an ecosystem-scale stomatal resistance by multiplying by leaf area index (LAI) and converting units to m s^{-1}

$$g_s = \mathrm{LAI}\frac{RT}{P}\left(g_0 + 1.6\left(1 + \frac{g_1}{\sqrt{D_s}}\right)\frac{A}{c_s}\right) \tag{3}$$

While Equation 3 can be used in PM, it will make analytical work with the function intractable because A is a function of ET itself. To remove dependence of ET on A we can use the semi-empirical results of **?**. **?** showed that:

$$uWUE = \frac{GPP \cdot \sqrt{D}}{ET} \tag{4}$$

is relatively constant across time and space (within plant functional type). If, following **?**, we approximate g_0 as 0, we can use uWUE to remove A from g_s in a way that makes PM analytically tractable:

$$g_s = \frac{RT}{P} 1.6 \left(1 + \frac{g_1}{\sqrt{D_s}}\right) \frac{uWUE\ ET}{c_s\ \sqrt{D}} \tag{5}$$

Note that $uWUE$ is fit on the ecosystem scale in **?** so GPP in 4 is really $A \cdot$ LAI. This leads to the cancelation of LAI in addition to uWUE in Equation 3. Plugging Equation 5 into Equation 1 and rearranging gives:

$$ET = \frac{\Delta R + \frac{g_a\ P}{T}\left(\frac{c_p D_s}{R_{air}} - \frac{\gamma c_s \sqrt{D}}{R* 1.6\ \text{uWUE}\ (1+\frac{g_1}{\sqrt{D}})}\right)}{\Delta + \gamma} \tag{6}$$

Given FLUXNET data described in Section 2, every term in Equation 6 is known. However, our sampling of sites and our focus on the growing season may intoduce some deviations of $uWUE$ from those observed in **?**. Also, we wish to include some measure of uncertainty in our analysis to guide if our many assumptions and simplifications are reasonable. To account for both mean deviations of $uWUE$ and uncertainty, we will introduce an uncertainty parameter σ modifying $uWUE$:

$$ET = \frac{\Delta R + \frac{g_a\ P}{T}\left(\frac{c_p D_s}{R_{air}} - \frac{\gamma c_s \sqrt{D}}{R* 1.6\ \sigma\ \text{uWUE}\ (1+\frac{g_1}{\sqrt{D}})}\right)}{\Delta + \gamma} \tag{7}$$

Now, from each FLUXNET observation we can calculate single value of σ:

$$\sigma = -\frac{g_a \gamma c_s \sqrt{D_s} L_v P}{\left(\text{ET}\ (\Delta + \gamma) - \Delta R - g_a \rho_a c_p D_s\right) 1.6\ R\ T\ \ \text{uWUE}\ (1 + \frac{g_1}{\sqrt{D_s}})} \tag{8}$$

The variablility of σ across sites and time will provides some measure of uncertainty in our model, assumptions, as well as the fluxnet observations themselves. Mean shifts in σ can be attributed to differences in out sampling from those used to calcualte $uWUE$ in **?**. The influence of σ will propogate through any uncertainty to our derivative of Equation 8:

$$\frac{\partial\ ET}{\partial\ D} = \frac{2\ g_a\ P}{T(\Delta+\gamma)}\left(\frac{c_p}{R_{air}} - \frac{\gamma c_s}{1.6\ R*\ \sigma\ \text{uWUE}}\left(\frac{2g_1+\sqrt{D}}{2(g_1+\sqrt{D})^2}\right)\right) \tag{9}$$

With Equation 9 we have provided an analytical franework for ecosystem reponse to atmospheric demand perturbations. There are a few subtelties to taking the derivative in Equation 9: Δ ($\frac{de_s}{dT}$) and D are functionally related, so while taking the derivative we evaluate $\frac{\partial\ ET}{\partial\ D} = \frac{\partial\ ET}{\partial\ e_s}\frac{\partial\ e_s}{\partial\ D}\Big|_{\text{RH fixed}} + \frac{\partial\ ET}{partial\ RH}\frac{\partial\ RH}{\partial\ D}\Big|_{e_s\ \text{fixed}}$. RH and e_s are assumed to be approximately orthogonal.

The D dependence in Equation 9 is a little opaque. However, mean D is 1062 Pa, so $\sqrt{D}$ is 32.6 $\text{Pa}^{1/2}$, which is much less than g_1 (with the exception of ENF; Table 3). So a series expansion in the limit $\frac{\sqrt{D}}{g_1} \to 0$ gives an approximation which makes the functional form more clear:

← Should I even include the series expansion?

$$\frac{\partial\ ET}{\partial\ D} \approx \frac{g_a\ P}{T(\Delta+\gamma)}\left(\frac{c_p}{R_{air}} - \frac{\gamma c_s}{1.6\ R*\ \sigma\ \text{uWUE}}\left(\frac{1}{g_1} - \frac{3\sqrt{D}}{2g_1^2} + \frac{2\sqrt{D}^2}{g_1^3} - \frac{5\sqrt{D}^3}{2g_1^4} + O\left(\left(\frac{\sqrt{D}}{g_1}\right)^4\right)\right)\right) \tag{10}$$

One final comment on our derivation which will not be discussed further but is relevant for future analysis: if we approximage c_s at a global mean CO_2 concentration, then the RHS of Equation 6 is fully defined using commonly available weather station data and the constants published in **??**. This then begs the question, why use PET for drought metrics in vegetated areas? It appears a much more physically realistic estimate of ET can be had with the same information reqiured to calculate PET.

We restrict our analysis to the daytime (sensible heat > 5 W m^{-1} and shortwave radiation > 50 W m^{-2}) when there is no precipitation and the plants are growing (GPP > 10% of the 95th percentile) . Also, because some sites use half hourly data but some use hourly, we aggregate all data to hourly averages. Only times with good quality control flags are used.

← This GPP thresholding was used by Changjie, do you know if there is a citation for it? Otherwise it seems like something a reviewer would have issue with as it is arbitray

4 Results

By construction, the variability in the σ term (Equation **??**) contains all model and observational uncertainties. For an observation that perfectly matches our model and assumptions σ will be one. Therefore, if for our assumptions and framework to be reasonable σ should be $O(1)$. Figure 2 presents the histogram of calculated σs with outliers (lowest and

104 **Table 1.** Definition of symbols and variables

Variable	Description	Units
e_s	saturation vapor pressure	Pa
T	temperature	K
Δ	$\frac{\partial e_s}{\partial T}$	Pa K^{-1}
R	net radiation at land surface minus ground heat flux	W m^{-2}
g_a	aerodynamic conductance	m s^{-1}
ρ_a	air density	kg m^{-3}
c_p	specific heat capacity of air at constant pressure	J K^{-1} kg^{-1}
D	VPD	Pa
γ	psychrometric constant	Pa K^{-1}
g_s	stomatal conductance	m s^{-1}
g_{l-s}	leaf-scale stomatal conductance	mol m^{-2} s^{-1}
$R*$	universal gas constant	J mol^{-1} K^{-1}
LAI	leaf area index	-
σ	uncertainty parameter	-
c_s	CO_2 concentration	μ mol CO_2 mol^{-1} air

[a]Footnote text here.

105 **Table 2.** Plant functional types, their abbreviation, Medlyn coefficient [from **?**], and uWfUE [from **?**].

106 Note that units are converted such that the quantities fit into Equations 1-8 with the variables in Table 1.

Abbreviation	PFT	g_1 ($Pa^{0.5}$)	uWUE (μ-mol [C] $Pa^{0.5}$ J^{-1} [ET])
CRO	cropland	183.1	3.80
CSH	closed shrub	148.6	2.18
DBF	deciduous broadleaf forest	140.7	3.12
ENF	evergreen needleleaf forest	74.3	3.30
GRA	grassland (C3)	166.0	2.68

[a]Footnote text here.

highest 5% percent) and nonphysical values ($\sigma < 0.$) removed. All remaining σ values are $O(1)$ which provides confidence in model framework.

An additional concern is that the σ term may in fact be some function of D, in which case the dependence would need to be accounted for when taking the derivative. Figure 3 plots the joint distribution of σ and VPD, and shows that σ is very weakly a function of VPD. Given this weak dependence, we argue that Equation 9 is a valid approximation for ET response to D.

Before calculating the sensitivity of ET to VPD, it is useful to consider the functional form of Equation 9. There are three terms: a scaling term for the full expression we will call Term 1 ($\frac{g_a\ P}{T(\Delta+\gamma)}$), a relatively constant offset we will call Term 2 ($\frac{c_p}{R_{air}}$), and a variable term we will call Term 3 ($\frac{\gamma c_s}{1.6\ R\ \text{uWUE}}\left(\frac{2g_1+\sqrt{D}}{2(g_1+\sqrt{D})^2}\right)$). All variables are positive, so the relative magnitude between Term 2 and Term 3 will determine the sign of the derivative, while Term 1 will scale the expression larger or smaller.

Term 2 minus Term 3's role in determining the sign of the sensitivty of ET to VPD makes it crucuial for answering our question "When does VPD drive or reduce ET?" Exploring these terms more, c_s and γ variability is relatively less than σ and D variability, so variability within PFT will be solely determined by σ and D. If we fix uncertainty σ at PFT averages, then Term 2 minus Term 3 is just a function of D. We can further dertmine a D_{crit} where $\frac{\partial\, ET}{\partial\, D} = 0$:

$$D_{crit} = \frac{R_{air}}{4c_p}\left(\frac{\gamma c_s}{1.6\ R\ \overline{\sigma} uWUE} + \sqrt{\frac{\gamma c_s}{1.6\ R\ \overline{\sigma} uWUE}\left(\frac{\gamma c_s}{1.6\ R\ \overline{\sigma} uWUE} + 8g_1\frac{c_p}{R_{air}}\right)} - 4g_1\frac{c_p}{R_{air}}\right) \tag{11}$$

Values of D_{crit} as a function of PFT are shown in Table 4.

Figure 4 shows how (Term 2 - Term 3) varies with D and σ, as a function of PFT. Equation 10 aids interpretation of Figure 4. Larger $uWUE$, $\overline{\sigma}$, and $g1$ shift the leading-order constant term ($\frac{1}{g_1}$) towards smaller values, and (Term 2 - Term 3) towards positive values. $uWUE$ and $g1$ are both water-use effiency type constants. Higher values corresponde to plants that are more willing to spend water on primary production and less evolved to conserve water. Figure 4 confirms our physical intuition: CROs are the least water conservative so have the smallest constant portion of Term 3, while CSH are the most water conservative and have the largest constant portion of Term 3. For the VPD-dependent terms in Equation

Table 3. Values of D_{crit}, where $\frac{\partial ET}{\partial D} = 0$, evaluated at PFT average values for R_{air}, σ, γ, and c_s. For reference, these values are also provided.

PFT	R_{air}	c_s (ppm)	γ	$\overline{\sigma}$	$\overline{\sigma} \cdot uWUE$	D_{crit} **(Pa)**
CRO	288.680920	372.567691	65.351523	0.684394	2.602873	**133.165438**
CSH	289.067152	381.593622	67.613172	0.997224	2.175278	**4439.564212**
DBF	288.624437	377.449849	63.421812	0.881061	2.746393	**888.773243**
ENF	288.183849	377.676463	61.559242	1.217892	4.015362	**978.084845**
GRA	288.425651	377.264645	61.598768	0.850869	2.281074	**1141.630778**

[a]Footnote text here.

10, differences in $g1$ between PFTs exert a greater influence than difference $uWUE$, as the power of $g1$ increases. Increasing $uWUE$ and $g1$ decreases the VPD-dependence, but $g1$ has the bigger effect due to its increasing powers. ENF ($g1 = 74.31$) has by far the largest VPD dependence of response, while CRO ($g1 = 183.1$) has the smallest VPD dependence.

Figure 4b shows the location of the minima of ET, as a function of σ and D. For any σ or VPD less (more) than these curves, Term 2 - Term 3 will be negative (positive). It is clear that the portion of VPD observations below/above these curves will be a strong function of σ. However, we can see some general trends. For CSH, $\frac{\partial ET}{\partial D}$ should be negative for the vast majority of observed σ and VPD. The fraciton of positive $\frac{\partial ET}{\partial D}$ appears to be more even for ENF, GRA, and DBF, and we might expect a greater frequency of positive $\frac{\partial ET}{\partial D}$ for CRO.

In Term 1, $\frac{P}{T} \propto \rho$, so this should vary little relative to aerodynamic conductance and Δ. γ should also be relatively constant, so the scaling term, Term 1, should be primarily a function of aerodynamic conductance and temperature (through the function Δ). This makes sense, as aerodynamic conductance represents how efficently response at the surface is communicated to the atmosphere. As it increases, any plant response will be communicated more strongly to the atmosphere (and vice-versa).

Δ's presence in the scaling term also matches physical intition. Evaporative cooling will dampen the ability of the atmosphere to take more moisture, as e_s decreases with temperature. The decrease in e_s is proportional to Δ ($\delta e_s = \Delta \delta T$). So as Δ increases, you will get a larger damping of ET due to evaporative cooling. The functional from of Δ will be the

same across PFT, but the temperature range may vary slightly. In contrast, aerodynamic conductance will vary strongly with PFT due to the importance of surface roughness. So most of the differences in scaling between PFT should be in the aerodynamic conductance term. One interesting side note is that the coefficient of variability for both aerodynamic conductance and Term 1 is relatively constant across PFT, suggesting that the influence of aerodynamic conductance on the relative (to the PFT mean) variability of Term 1 is approximately similar across PFT.

Figure 5A shows Term 1 normalized by mean aerodynamic conductance (calculated for each plant functional type), and confirms that much of the relative variability of Term 1 is contained in the aerodynamic conductance variability. Generally, T has less of a role. Additionally, the impact of T on the relative variability increases with increasing aerodynamic conductance. .

← plot every PFT and show they collapse onto the same curve? - might just be too messy though

While the relative variability of Term 1 is similar across PFT, the absolute value of Term 1 varies strongly across PFT. Figure 5B shows Term 1 evaluated with the mean aerodynamic conductance for each PFT, and at the range of observed temperatures for each PFT. As expected, for the tree PFTs (DBF, ENF) Term 1 is much larger and the temperature dependence is much stronger. Systematic differences in observed temperatures also cause differences in the average magnitude of Term 1. For example, ENF experiences on average colder temperatures and is thus more likely to have a larger scaling term. Additionally, because the variability of aerodynamic conductance increases proportionally to the mean, the spread of Term 1 due to aerodynamic conductance variability will be larger for the tree PFTs, although this is not shown for simplicity. To summarize, the variability of Term 1 within each PFT will look like Figure 5A for each PFT, but the scale of the y-axis will increase or decrease according to mean aerodynamic conductance oberved in Figure 5B.

Table 3 confirms these expectations for PFT behavior of $\frac{\partial ET}{\partial D}$. For all PFTs except for CRO, average $\frac{\partial ET}{\partial D}$ is less than zero. However, $\frac{\partial ET}{\partial D}$ evaluated at the average of all variables (e.g. σ, T, c_s, D) is only negative for CSH and GRA. And, DBF in addition to CRO experiences $\frac{\partial ET}{\partial D} < 0$ less than half the time. These observations highlight the effect of the nonlinear function in Figure 4: $\frac{\partial ET}{\partial D}$ has a much steeper slope when the function is negative, and is thus more likely to be large.

The units of $\frac{\partial ET}{\partial D}$ make it difficult to interpret if D is even a meaningful contributor to ET's variability. To better understand D's contribution, we normalize $\frac{\partial ET}{\partial D}$ with D's standard

Table 4. Statistics of $\frac{\partial ET}{\partial D}$ as a function of PFT.

PFT	$\overline{\frac{\partial ET}{\partial VPD}}$	$\frac{\partial ET}{\partial D}\left(\overline{T,\ldots,D}\right)$	$\frac{\partial ET}{\partial D}\left(\overline{T,\ldots,D}\right) * \text{std}(D)$	$\frac{\frac{\partial ET}{\partial D}(\overline{T,\ldots,D})*\text{std}(D)}{\frac{\partial ET}{\partial R}(\overline{T,\ldots,D})*\text{std}(R)}$	fraction $\frac{\partial ET}{\partial VPD} < 0.$
CRO	0.000853	0.026241	18.523659	0.203022	0.473311
CSH	-0.108234	-0.091526	50.861613	0.439379	0.931660
DBF	-0.012727	0.013794	19.734435	0.164241	0.461674
ENF	-0.034087	0.000706	16.611852	0.148548	0.534425
GRA	-0.019637	-0.000921	16.798083	0.173552	0.631735

[a]Footnote text here.

deviation to define a (linearized) relative change in ET for variations in D . D's contribution to ET's variability ranges between 16 - 20 W m^{-2} for all PFTs except for CSH, which is about 51 W m^{-2}. Another meaningful comparison is to $\frac{\partial ET}{\partial R} * std(R)$, as net radiationis generally the driver of ET (cite joe berry here). For all PFTs except for CSH D contributes between 14.5 - 20.5 % of R's contribution to variability. For CSH the portion is much larger, about 44 %. D's variability is certiantly a non-negligable contributor to ET's variability.

So far, idealized plots and statistics have illuminated the form of $\frac{\partial ET}{\partial D}$ and how it varies with PFT. Large mean σ and uWUE shifts CRO and DBF towards positive $\frac{\partial ET}{\partial D}$. However, the strongly nonlinear function of $\frac{\partial ET}{\partial D}$ at $\frac{\partial ET}{\partial D} < 0$ pushes $\overline{\frac{\partial ET}{\partial D}}$ negative for DBF (it does not do this for CRO because of CRO's high $g1$). ENF's low $g1$ value increases the dependence of $\frac{\partial ET}{\partial D}$ on D, and makes the function more strongly nonlinear. This has the side effect of pushing $\overline{\frac{\partial ET}{\partial D}}$ negative further than other PFTs for a given fraction $\frac{\partial ET}{\partial D} < 0$ and magnitude $\frac{\partial ET}{\partial D}(\overline{T,\ldots,D})$. GRA shows the opposite behavior; a relatively high $g1$ makes the function more linear, decreasing the magnitude of $-\overline{\frac{\partial ET}{\partial D}}$ for a given [large] fraction $\frac{\partial ET}{\partial D} < 0$ and negative $\frac{\partial ET}{\partial D}(\overline{T,\ldots,D})$ (although aerodynamic conductance and Term 1 also probably have a role in this). Finally, low $uWUE$ of CSH pushes to toward by far the lowest values $\frac{\partial ET}{\partial D}$ (Figure 4). Variability in D accounts for the largest about of ET variability for CSH. For the other PFTs, D contributes less to ET variability, but still represents about 15-20 % of R's contributions to ET variability.

4.1 Full observations of $\frac{\partial ET}{\partial D}$

Now that we have an intuitive understanding of $\frac{\partial ET}{\partial D}$'s behavior, we are equipped to interpret fully realistic plots of $\frac{\partial ET}{\partial D}$ for each PFT. Figure 6 presents calculated $\frac{\partial ET}{\partial D}$ where, unless otherwise noted, all variables in Equation 9 are allowed to vary. Each column is a different quantity related to $\frac{\partial ET}{\partial D}$, and each row is a different PFT.

The full observations generally confirm expectations from Section 4. CRO has the most positive values of $\frac{\partial ET}{\partial D}$, $\frac{\partial ET}{\partial D}$ is almost always negative for CSH, and response depends more with the environmental conditions for the other PFTs (especially ENF). Through the columns of Figure 6 we can see the impact of σ and g_a on the variability of $\frac{\partial ET}{\partial D}$. g_a's scaling (included in columns 1 and 3) alters the magnitude considerably. σ variability (included in columns 1 and 2) adds a lot of additional noise to the signal of $\frac{\partial ET}{\partial D}$, which is slightly undesirable given σ's role in representing model and observational uncertainty. However, the general story with the noise appears to match the cleaner signal when σ is help constant and D_{ETmin} is clearly visible . One exception is possibly with GRA, for which uncertainty represented in σ is high and causes the full complexity plots (Columns 1 and 2) to not match well with σ held fixed (Columns 3 and 4).

← I really need to make these plots better - way too much overlapping of points that hurts the story

For ENF and GRA D_{ETmin} does not appear to be only a function of σ (most observable in Column 4). It turns out that the site to site variability in γ causes D_{ETmin} to vary, which is not discussed in the previous section. The impact is observable in both ENF and GRA, but especially for ENF which has a larger $\frac{\partial^2 ET}{\partial^2 D}$ than the other PFTs.

In general the full complexity plots of $\frac{\partial ET}{\partial D}$ match our expectations, even with the large sensitivity to σ measures of uncertainty observed in Figure 4. Our σ-based method of uncertainty propagation blurs the idealized expectations the most for GRA, and also has a considerable effect for CRO. We therefor have the most confidence in our conclusion based on Equation 9 for PFTS CSH, DBF, and ENF, as the full complexity plots with uncertainty included closely match the story when σ is held fixed. **see somewhat preferred alternate figure 7 .

← I think I like the alternate plot much more as thinking in terms of T and RH is easier, and it makes the story easier to see at relatively low temperatures. However, I used the other plot because Fig 5 does not discuss things in terms of

5 Conclusions

The idealized representation of ET used here is successful in developing intuition for how ET responds to changes in D. This intuition will aid the community in interpreting observations and output from sophisticated full complexity climate models.

The idealized framework leads to the following general conclusions:

- Aerodynamic resistance plays an important role of scaling $\frac{\partial ET}{\partial D}$. This is a leading order effect for observing higher magnitude responses in DBF and ENF.
- In general, CSH has the most negative (i.e. ET reduced) response to increases in D (atmospheric drying). So CSH plants will almost always try and conserve water, effectively reducing ET with dry atmospheric perturbation.
- Additionally for CSH, D variability contributes the most to ET variability.
- CRO has the most positive response (i.e. ET increased) in response to increases in D. This is consistent with CROs that may be evolved or bred to thrive in non-water-limited environments.
- The response is more a function of the environment for DBF, ENF, and GRA. Because as VPD increases the response is more likely to be positive, if RH is fixed then the response will be more likely to be positive at warmer T, or if T is fixed the response is more likely to be positive with decreasing RH.
- ENF has the strongest dependence on environmental conditions due to its small $g1$.
- Model and observational uncertainty is highest for GRA and CRO, so conclusions about those PFTs should be tempered.
- However, inclusion of uncertainty doesn't alter conclusions about DBF, ENF, and CSH.

The intuition developed using this framework can be used to understand how the land surface will respond and contribute to changes in the environment. Additionally, Equation 6 gives provides an estimate of ET that requires no additional information beyond that required to calculate PET. Given that for all PFTs, with the exception of CRO, we found a high frequency and magnitude of negative $\frac{\partial ET}{\partial D}$, PET is a physically unrealisitic representation of ET for vegetated surfaces and PET-based drought metrics are not usefull. We advocate for drought metrics using Equation 6 instead of PET.

Acknowledgments

This work used eddy covariance data acquired and shared by the FLUXNET community, including these networks: AmeriFlux, AfriFlux, AsiaFlux, CarboAfrica, CarboEuropeIP, CarboItaly, CarboMont, ChinaFlux, Fluxnet-Canada, GreenGrass, ICOS, KoFlux, LBA, NECC, OzFlux-TERN, TCOS-Siberia, and USCCC. The ERA-Interim reanalysis data are provided

by ECMWF and processed by LSCE. The FLUXNET eddy covariance data processing and harmonization was carried out by the European Fluxes Database Cluster, AmeriFlux Management Project, and Fluxdata project of FLUXNET, with the support of CDIAC and ICOS Ecosystem Thematic Center, and the OzFlux, ChinaFlux and AsiaFlux offices.

References

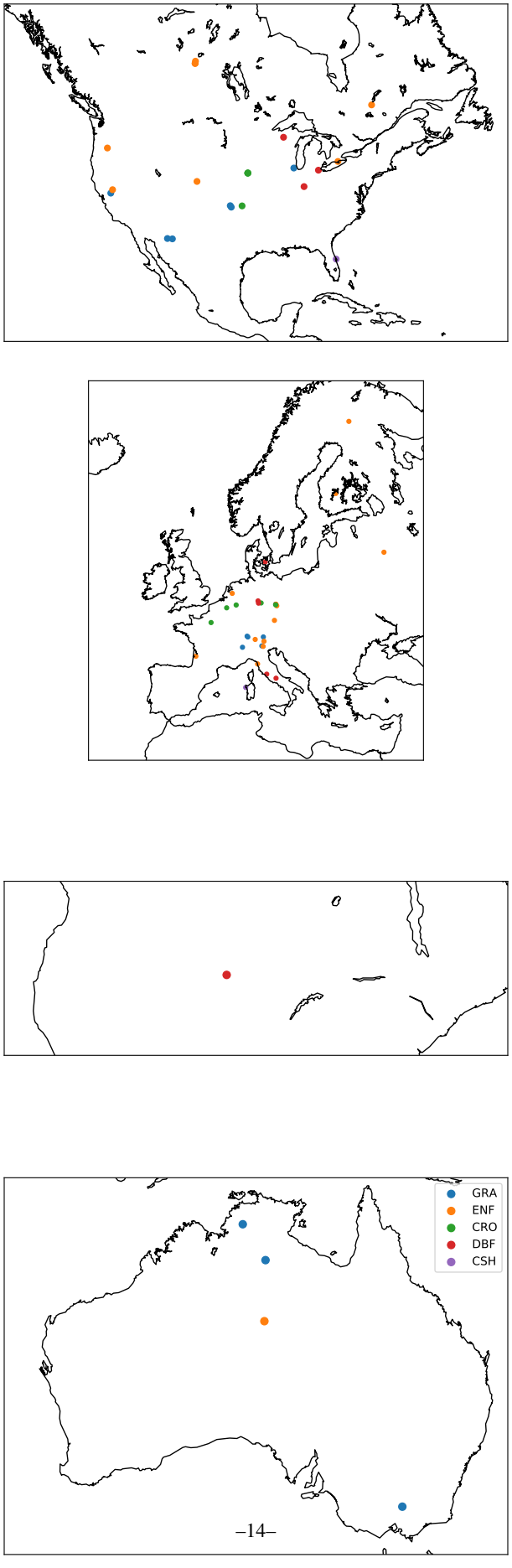

Figure 1. Plant functional type and location of sites used in analysis. ***This is just a placeholder for now and needs to be improved i.e. with lat lon, better placement of continents, etc.)***

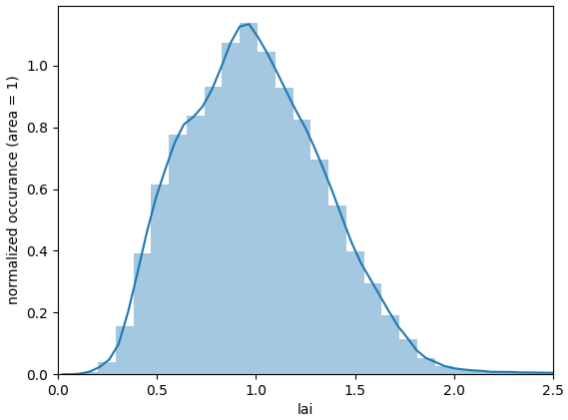

Figure 2. Histogram of σ values calculated for each site and time according to Equation **??**. The lowest and highest 5% are removed as outliers, as well as any values below 0. The curve is normalized such that its area is 1.

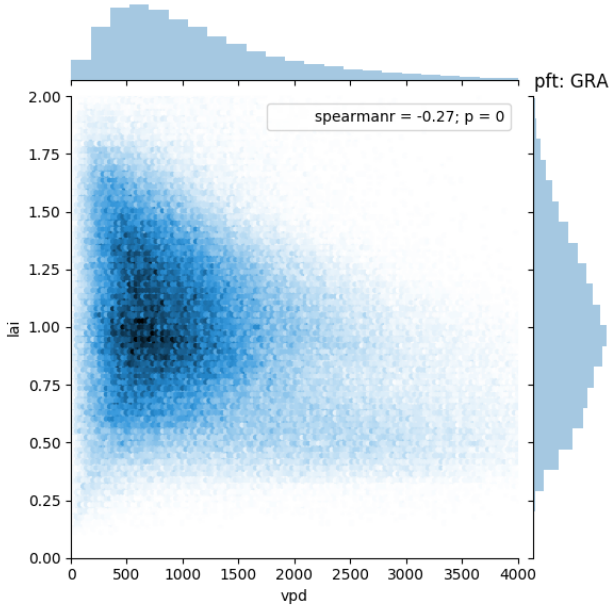

Figure 3. The joint distribution of D and σ. σ has only a weak dependence on D. ***This plot could proabably benefit from a box plot of site specific correlations, because some sites do have stronger deped-nence than others. Note also Figs 3 and 2 can probably be combined because this figure shoes σ's his-togram.***

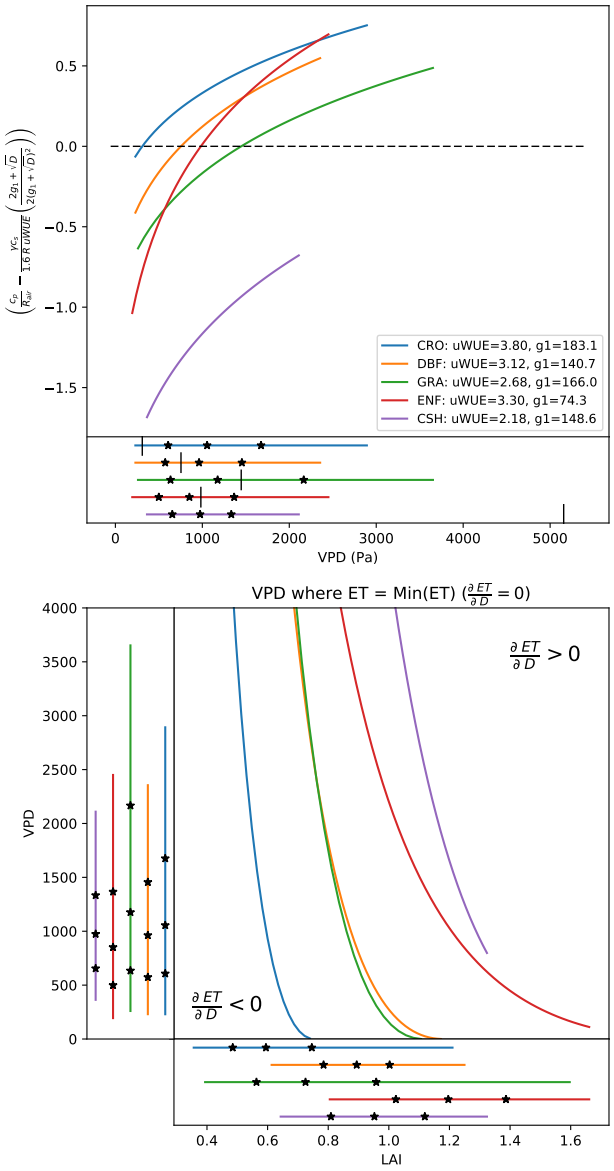

Figure 4. Sources of variability for Term 2 - Term 3. Top: Term 2 - Term 3 as a function of VPD, with σ held fixed at PFT averages. The observed range of VPD for each PFT is also shown below the x-axis. Line extent corresponds to 5th and 95th percentiles, while stars denote the location of the 25th, 50th, and 75th percentiles.

Bottom: The location of the minima of ET, as a function of VPD and σ. Lines and stars denote the distribution of VPD and σ next to each axis, following the same percentiles as above.

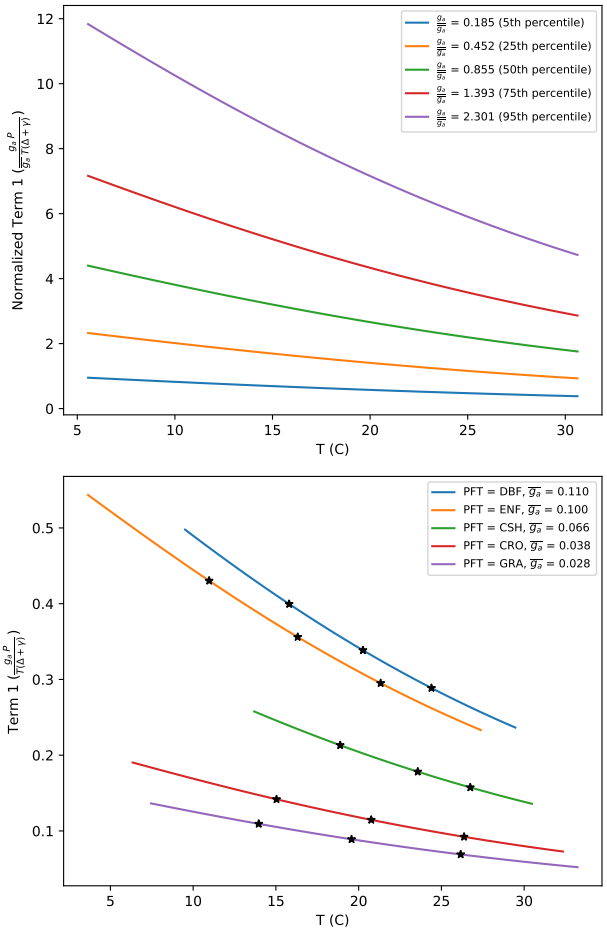

Figure 5. Primary sources of variability for Term 1. A) Variability within each PFT: Term 1 normalized by mean g_a for each PFT. B) Variability between each PFT: Term 1 evaluated at mean g_a for each PFT. Temperature range is 5-95th percentile for each PFT. Additionally, stars denote the location of the 25th, 50th, and 75th percentiles.

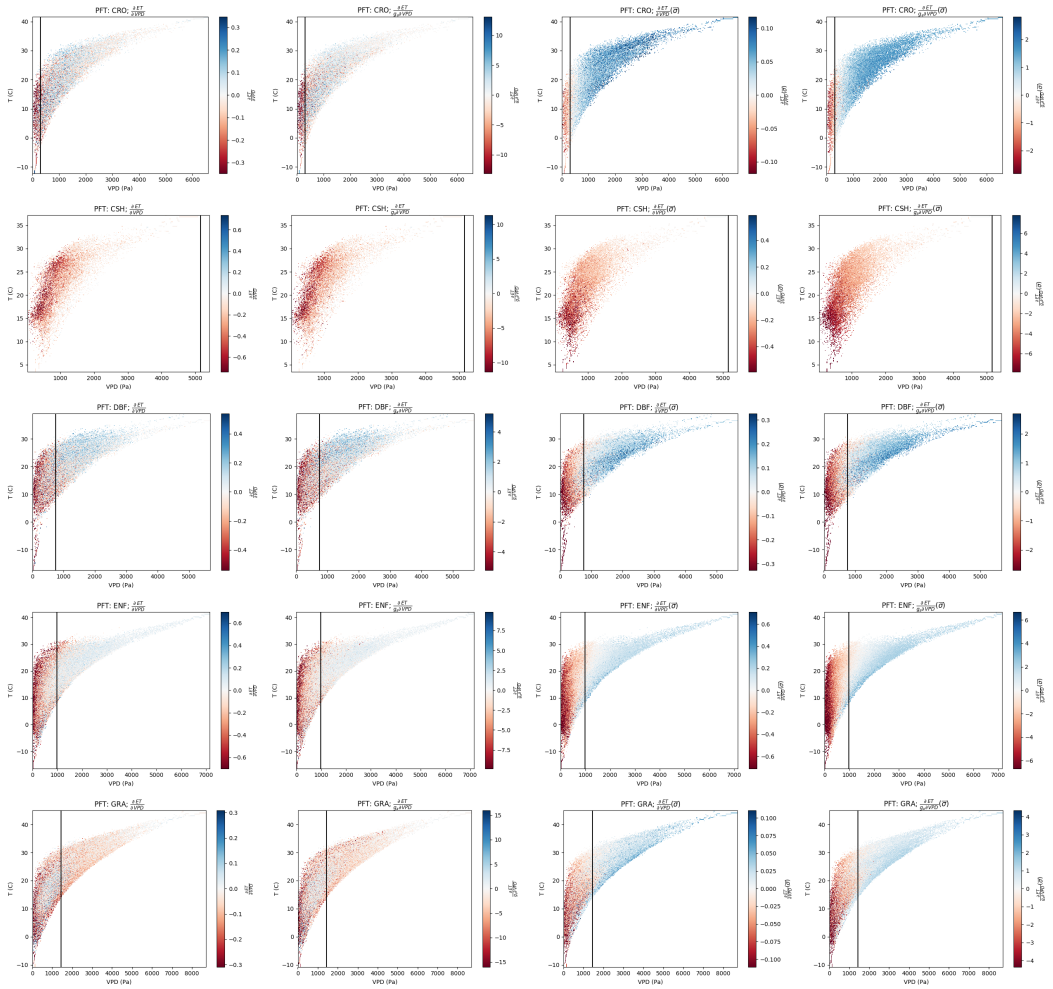

Figure 6. Scatter plots of $\frac{\partial ET}{\partial D}$. Each row is a different PFT, and each column is a different quantity related to $\frac{\partial ET}{\partial D}$, as labeled: Column 1 - $\frac{\partial ET}{\partial D}$; Column 2 - $\frac{\partial ET}{\partial D}$ normalized by g_a; Column 3 - $\frac{\partial ET}{\partial D}$ with σ held fixed at PFT average; and Column 4 - $\frac{\partial ET}{\partial D}$ normalized by g_a and with σ held fixed. For reference, lines corresponding to RH = 20% and RH = 90 % are drawn. Please note differences in the colorbar scale. ***see alternate (or additional) plot below.***

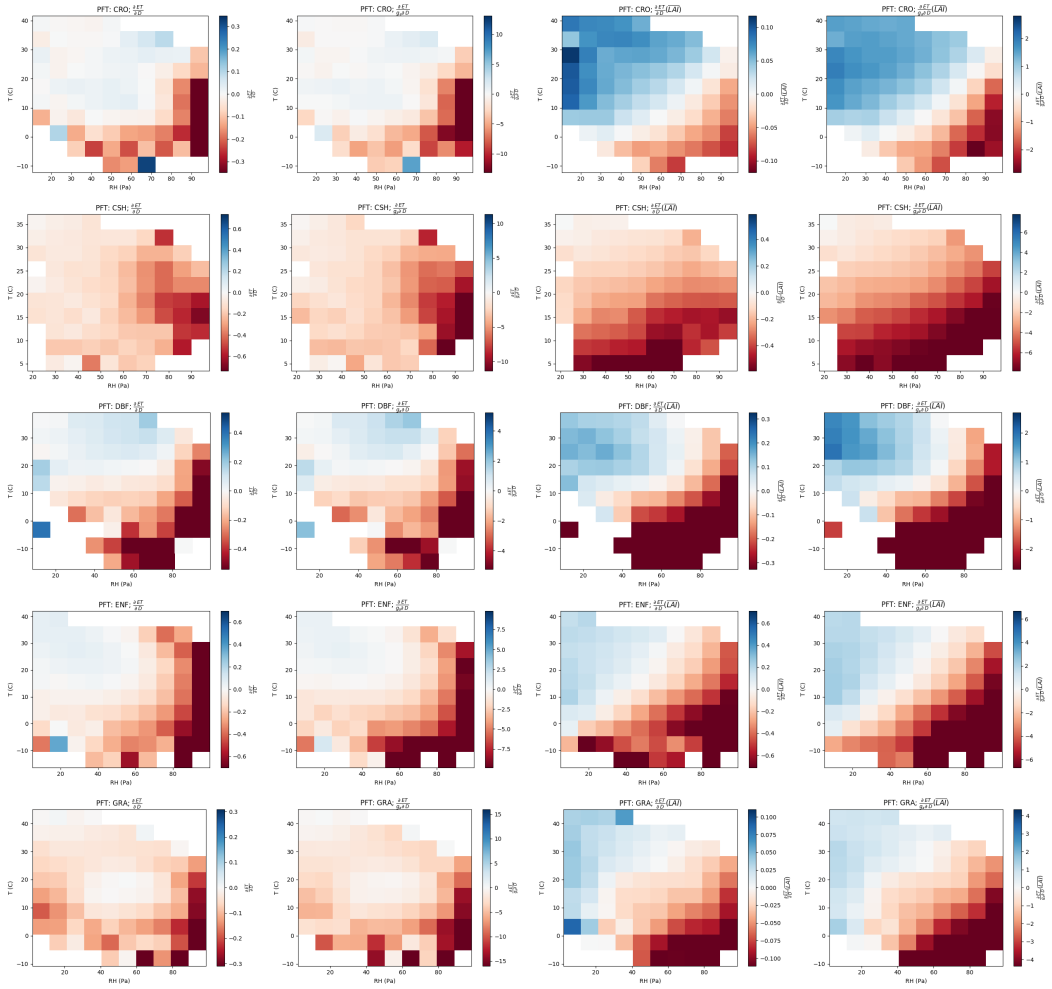

Figure 7. ****alternate Fig 06**** Scatter plots of $\frac{\partial ET}{\partial D}$. Each row is a different PFT, and each column is a different quantity related to $\frac{\partial ET}{\partial D}$, as labeled. If I end up using this, I could also draw on the curve of D_{ETmin} with $\frac{\overline{\text{LAI}}}{\text{LAI}_{ref}}$.